fluids

MDPI

Article

Investigation of Nonlinear Relations Among Flow Profiles Using Artificial Neural Networks

Shiming Yuan [1], Caixia Chen [1], Yong Yang [2,*] and Yonghua Yan [1]

[1] Department of Mathematics and Statistical Sciences, Jackson State University, Jackson, MS 39217, USA; shiming.yuan@students.jsums.edu (S.Y.); caixia.chen@jsums.edu (C.C.); yonghua.yan@jsums.edu (Y.Y.)
[2] Department of Mathematics, West Texas A&M University, Canyon, TX 79016, USA
* Correspondence: yyang@wtamu.edu

Abstract: This study investigated the ability of artificial neural networks (ANNs) to resolve the nonlinear dynamics inherent in the behavior of complex fluid flows, which often exhibit multifaceted characteristics that challenge traditional analytical or numerical methods. By employing flow profile pairs that are generated through high-fidelity numerical simulations, encompassing both the one-dimensional benchmark problems and the more intricate three-dimensional boundary layer transition problem, this research convincingly demonstrates that neural networks possess a remarkable capacity to effectively capture the discontinuities and the subtle wave characteristics that occur at small scales within complex fluid flows, thereby showcasing their robustness in handling intricate fluid dynamics phenomena. Furthermore, even in the context of challenging three-dimensional problems, this study reveals that the average velocity profiles can be predicted with a high degree of accuracy, utilizing a limited number of input profiles during the training phase, which underscores the efficiency and efficacy of the model in understanding complex systems. The findings of this study significantly underscore the immense potential that artificial neural networks, along with deep learning methodologies, hold in advancing our comprehension of the fundamental physics that govern complex fluid dynamics systems, while concurrently demonstrating their applicability across a variety of flow scenarios and their capacity to yield insightful revelations regarding the nonlinear relationships that exist among diverse flow parameters, thus paving the way for future research in this critical area of study.

Keywords: artificial neural networks; velocity profiles; complex flows

Citation: Yuan, S.; Chen, C.; Yang, Y.; Yan, Y. Investigation of Nonlinear Relations Among Flow Profiles Using Artificial Neural Networks. *Fluids* **2024**, *9*, 276. https://doi.org/10.3390/fluids9120276

Academic Editor: Robert Martinuzzi

Received: 4 September 2024
Revised: 12 November 2024
Accepted: 22 November 2024
Published: 23 November 2024

1. Introduction

The investigation of complex fluid flows, which are characterized by their nonlinear dynamics and multifaceted interactions, has long been a pivotal area of inquiry within the realm of fluid dynamics research. Traditional numerical methods, while robust and widely utilized, frequently encounter significant challenges in accurately capturing the intricate complexities associated with nonlinear behaviors, particularly in scenarios that involve shock waves, discontinuities, and transitional flow phenomena. This limitation is compounded by the increasing demand for computationally efficient flow simulations that can address fluid-related problems without the prohibitive costs associated with conventional fluid mechanics approaches.

The advent of artificial neural networks (ANNs) [1–5] offers a promising avenue for overcoming these obstacles, as ANNs are adept at modeling the complex, nonlinear relationships that are intrinsic to dynamic systems. In recent years, a growing corpus of research has also emerged that investigates the utilization of ANNs for modeling fluid dynamics. For instance, Morimoto et al. [6] emphasized the importance of generalization techniques in neural networks for fluid flow estimation, highlighting the challenges associated with the need for extensive datasets and the difficulties of generalizing models

across varying flow conditions. Razdan and Shah [7] provided a comprehensive review of the optimization of fluid modeling and flow control processes through machine learning, detailing various methodologies and their applications across diverse fluid dynamics scenarios. Furthermore, Mendez et al. [8] delved into the challenges and opportunities presented by the integration of machine learning with fluid mechanics, addressing critical issues such as data requirements, model generalizability, and the implementation of physical constraints. Roy et al. [9] utilized Graph Network-based Simulators (GNSs) to solve complex fluid dynamics problems, achieving prediction accuracies of around 99% while generalizing well across different conditions. Khan et al. [10] demonstrated the ability of the NN-BLMM model to handle nonlinear partial differential equations and provided insights into non-Newtonian fluid behaviors by simulating magnetohydrodynamic stagnation point flows. Morra et al. [11] investigate hypersonic three-dimensional Navier–Stokes flow over a cone geometry, optimizing the training dataset and demonstrating that a neural network—surpassing a linear surrogate model in capturing nonlinearities—can be applied as a surrogate model to solve an inverse problem and reconstruct three-dimensional flow from experimental measurements.

However, the application of machine learning techniques to directly predict complex fluid flows (usually 3D) is still fraught with challenges, primarily due to the substantial volume of training data required. The acquisition of these data can prove to be a formidable task, particularly for complex flows that exhibit structures across a wide range of scales. At present, the computational resources and data availability required for direct predictions remain insufficient, creating a significant bottleneck in the development of effective predictive models. Moreover, the generalizability of neural networks presents an additional hurdle. A model that has been trained on a specific dataset may not perform adequately when applied to a different dataset, which is particularly problematic in complex flow scenarios (either with a complex domain or complex flow structures) where even minor changes in boundary conditions or within the flow field can lead to substantial alterations in the downstream flow characteristics. This sensitivity complicates the training of standard neural network models, as they may struggle to adapt to these dynamic changes.

Nevertheless, machine learning, particularly deep learning, has shown significant potential in addressing some of these challenges by efficiently predicting flow fields and offering an alternative to traditional computational fluid dynamics (CFD) methods. Convolutional Neural Networks (CNNs) have been employed to approximate steady-state fluid flows, demonstrating substantial reductions in computational cost while maintaining reasonable accuracy, though some trade-offs remain when compared to conventional solvers [12]. Recent advancements, such as DeepCFD, have refined CNN architectures, specifically optimizing laminar flow predictions with improved efficiency and data utilization [13]. The Physics-Informed Neural Network (PINN) integrates physical laws directly into the neural network's architecture, allowing for efficient and accurate simulations of fluid flows without the need for extensive labeled datasets [14]. Additionally, alternative neural network structures are being explored to predict more complex and turbulent flows, addressing the nonlinearity and multi-scale nature inherent in these regimes [15]. While these approaches offer promising advancements, challenges still persist in balancing computational efficiency, accuracy, and generalizability, especially for flows that span diverse physical conditions.

On the other hand, there has been limited research on the ability of machine learning methods to resolve or understand the underlying dynamics in various fluid flows. Overly complex models may overfit sparse data, leading to poor generalization, while overly simplistic models may fail to capture essential physical phenomena. There is a need to evaluate the capability of machine learning methods, especially artificial neural networks, in understanding complex fluid dynamics involving discontinuities and small-scale structures. When given some information about the characteristics of the fluid motion (such as a set of velocity profiles obtained from experiments or calculations), can machine learning predict the overall picture of the flow field (other motion characteristics)? This will help subsequent

research, which is committed to using machine learning on a larger scale to reduce the existing amount of computation and obtain more flow field information.

In this study, we employed a multilayer perceptron (MLP) artificial neural network to scrutinize the complex nonlinear dynamics exhibited in flow profiles derived from numerical simulations of compressible fluids. Our research focuses on the application of ANNs to enhance the understanding and prediction of nonlinear behaviors in complex fluid flows. By utilizing flow profile pairs generated from numerical simulations of canonical benchmark cases, such as the 1D Sod tube problem and the Shu–Osher problem, we aimed to capture essential features, including discontinuities and small-scale waves that are prevalent in complex flows. These benchmark cases provide a solid framework for evaluating the efficacy of ANNs in fluid dynamics applications.

Additionally, this study sought to explore how machine learning methodologies can enrich our comprehension of complex fluid dynamics phenomena. Through the analysis of averaged velocity profiles associated with boundary layer transition problems, we sought to uncover nonlinear correlations among various flow parameters within the context of the Navier–Stokes equations, thereby offering deeper insights into the fundamental physics at play. We underscore the capability of ANNs to elucidate nonlinear relationships among multiple flow variables, thereby demonstrating their potential for predicting the evolution of complex fluid flows.

The structure of this paper is organized as follows: Section 2 presents the mathematical foundations of the problems under investigation and the methodologies employed. In Section 3, we showcase the numerical results obtained from the 1D benchmark cases as well as the averaged velocity profiles derived from the 3D transition problem. Finally, Section 4 concludes with a summary of our findings and offers final reflections on the implications of our research.

2. Mathematical Background and Methodologies

2.1. One-Dimensional Benchmark Problems

A comprehensive grasp of compressible fluid dynamics is essential for a multitude of engineering and scientific applications, ranging from aerospace engineering to environmental studies. This intricate field encompasses a variety of complex scenarios, including the behavior of shock waves, which are abrupt changes in pressure and density, as well as boundary layer transitions that occur when fluid flow interacts with solid surfaces. To effectively analyze and predict these phenomena, researchers frequently turn to the one-dimensional Euler equations. These fundamental equations serve as a cornerstone in the mathematical modeling of compressible fluid behavior, encapsulating the principles of conservation of mass, momentum, and energy. Their applicability extends to a range of benchmark problems that are pivotal for validating numerical methods and theoretical approaches. Notably, the Sod shock tube problem provides a classic example of how shock waves propagate through a medium, enabling researchers to observe the dynamics of rarefaction and contact discontinuities. Similarly, the Shu–Osher problem offers insights into the interaction of shock waves with smooth density interfaces, serving as a critical test case for assessing the accuracy of computational fluid dynamics (CFD) algorithms. Through the study of these equations and associated benchmark problems, engineers and scientists can enhance their understanding of compressible flow phenomena, paving the way for advancements in technology and improved designs across various fields.

The one-dimensional Euler equation, expressed in vector and conservation form, is given as follows:

$$\frac{\partial}{\partial t}\begin{bmatrix}\rho\\ \rho u\\ E\end{bmatrix}+\frac{\partial}{\partial x}\begin{bmatrix}\rho u\\ \rho u^2+p\\ u(E+p)\end{bmatrix}=0 \tag{1}$$

where ρ, u, and E represent density, velocity, and total energy, respectively. p represents pressure and is calculated by $p=(\gamma-1)\left(E-\frac{1}{2}\rho u^2\right)$.

2.1.1. Sod Shock Tube Problem

The Sod shock tube problem [16] is a well-known example in computational fluid dynamics that models the dynamics of a shock wave moving through a tube filled with gas, which is initially divided by a diaphragm. Once the diaphragm is taken away, the resulting shock wave allows us to assess the precision of numerical techniques in representing shock wave behavior, including propagation, rarefaction waves, and contact discontinuities. It acts as a standard for evaluating the precision and effectiveness of numerical methods in representing shock wave phenomena, such as shock wave propagation, rarefaction waves, and contact discontinuities. The Sod shock tube problem has the following initial conditions defined:

$$\begin{bmatrix} \rho_L \\ p_L \\ u_L \end{bmatrix} = \begin{bmatrix} 1.0 \\ 1.0 \\ 0.0 \end{bmatrix}, \quad \begin{bmatrix} \rho_R \\ p_R \\ u_R \end{bmatrix} = \begin{bmatrix} 0.125 \\ 0.1 \\ 0.0 \end{bmatrix} \tag{2}$$

where the indices L and R denote conditions on the left- and right-hand sides, respectively, with the center located at $x = 0$.

2.1.2. Shu–Osher Problem

The Shu–Osher problem [17,18] constitutes a quintessential benchmark scenario within the realm of computational fluid dynamics, particularly within the framework of shock wave interactions. This problem entails the modeling of a one-dimensional compressible gas flow over a wedge, which leads to the generation of both shock waves and rarefaction waves. This challenge is named in honor of its creators, Chi-Wang Shu and Stanley Osher, and functions as a standard validation case for numerical methodologies intended to precisely resolve shock structures while effectively capturing intricate flow phenomena. This problem is particularly challenging due to the sensitivity of entropy waves to numerical dissipation, which may lead to excessive damping. The same governing Equation (1) is solved, with the initial conditions specified as follows:

$$\begin{bmatrix} \rho_L \\ p_L \\ u_L \end{bmatrix} = \begin{bmatrix} 3.857143 \\ 10.33333 \\ 2.629369 \end{bmatrix}, \quad \begin{bmatrix} \rho_R \\ p_R \\ u_R \end{bmatrix} = \begin{bmatrix} 1 + 0.2\sin(5x) \\ 1.0 \\ 0.0 \end{bmatrix} \tag{3}$$

where the indices L and R denote conditions on the left- and right-hand sides, respectively, with the center located at $x = 0$.

2.2. Transitional Boundary Layer

The transitional boundary layer is a critical region in fluid dynamics that lies adjacent to solid surfaces, where the flow transitions from a smooth, orderly laminar state to a chaotic, turbulent state. This boundary layer is of paramount importance in various engineering fields, including aerodynamics, heat transfer, and boundary layer control, as it significantly influences the performance and efficiency of aerodynamic surfaces, such as wings and fins, as well as heat exchangers used in thermal systems. In this transitional zone, the characteristics of the fluid flow undergo a profound transformation. Initially, the flow is laminar, marked by streamlined layers of fluid that glide past one another with minimal mixing and turbulence. However, as the flow progresses through this boundary layer, it begins to experience instabilities that disrupt the orderly arrangement of the laminar flow. This instability results in a gradual breakdown of the smooth flow patterns, leading to the development of turbulent fluctuations. These fluctuations are characterized by random, chaotic movements of fluid particles, which enhance mixing and energy transfer within the flow. The dynamics of the transitional boundary layer are complex and involve various physical phenomena, including changes in velocity gradients, pressure fluctuations, and the influence of surface roughness. Understanding these dynamics is crucial for engineers and researchers who seek to optimize design strategies for a wide range of applications. For instance, in aerodynamics, managing the transition from laminar to turbulent flow can

reduce drag on aircraft wings, thereby improving fuel efficiency and overall performance. In the realm of heat exchangers, effectively controlling the boundary layer can enhance heat transfer rates, leading to more efficient thermal management systems.

The Navier–Stokes equation in curvilinear coordinates was used in our DNS of the transitional boundary layer, as follows:

$$\frac{\partial \boldsymbol{Q}}{\partial t}+\frac{\partial \boldsymbol{F}}{\partial x}+\frac{\partial \boldsymbol{G}}{\partial y}+\frac{\partial \boldsymbol{H}}{\partial z}=\frac{1}{Re}\left(\frac{\partial \boldsymbol{F_v}}{\partial x}+\frac{\partial \boldsymbol{G}_v}{\partial y}+\frac{\partial \boldsymbol{H}_v}{\partial z}\right), \tag{4}$$

where the vector of conserved quantities $\boldsymbol{Q}$, inviscid flux vector $\boldsymbol{E}$, $\boldsymbol{F}$, and $\boldsymbol{G}$, and viscous flux vector $\boldsymbol{E}_v$, $\boldsymbol{F}_v$, and $\boldsymbol{G}_v$ are

$$\boldsymbol{Q}=\begin{pmatrix}\rho\\ \rho u\\ \rho v\\ \rho w\\ e\end{pmatrix},\ \boldsymbol{F}=\begin{pmatrix}\rho u\\ \rho u^2+p\\ \rho uv\\ \rho uw\\ (e+p)u\end{pmatrix},\ \boldsymbol{G}=\begin{pmatrix}\rho v\\ \rho uv\\ \rho v^2+p\\ \rho vw\\ (e+p)v\end{pmatrix},\ \boldsymbol{H}=\begin{pmatrix}\rho w\\ \rho uw\\ \rho vw\\ \rho w^2+p\\ (e+p)w\end{pmatrix}, \tag{5}$$

$$\boldsymbol{F}_v=\begin{pmatrix}0\\ \sigma_{xx}\\ \sigma_{xy}\\ \sigma_{xz}\\ (u\sigma_{xx}+v\sigma_{xy}+w\sigma_{xz}+\frac{1}{(\gamma-1)PrM_\infty^2}k(T)\frac{\partial T}{\partial x}\end{pmatrix}, \tag{6}$$

$$\boldsymbol{G}_v=\begin{pmatrix}0\\ \sigma_{xy}\\ \sigma_{yy}\\ \sigma_{yz}\\ (u\sigma_{xy}+v\sigma_{yy}+w\sigma_{yz}+\frac{1}{(\gamma-1)PrM_\infty^2}k(T)\frac{\partial T}{\partial y}\end{pmatrix}, \tag{7}$$

$$\boldsymbol{H}_v=\begin{pmatrix}0\\ \sigma_{xz}\\ \sigma_{yz}\\ \sigma_{zz}\\ (u\sigma_{xz}+v\sigma_{yz}+w\sigma_{zz}+\frac{1}{(\gamma-1)PrM_\infty^2}k(T)\frac{\partial T}{\partial z}\end{pmatrix}. \tag{8}$$

The components of viscous stress are

$$\begin{gathered}\sigma_{xx}=\tfrac{2}{3}\mu(T)\left(2\tfrac{\partial u}{\partial x}-\tfrac{\partial v}{\partial y}-\tfrac{\partial w}{\partial z}\right),\ \sigma_{yy}=\tfrac{2}{3}\mu(T)\left(-\tfrac{\partial u}{\partial x}+2\tfrac{\partial v}{\partial y}-\tfrac{\partial w}{\partial z}\right),\\ \sigma_{zz}=\tfrac{2}{3}\mu(T)\left(-\tfrac{\partial u}{\partial x}-\tfrac{\partial v}{\partial y}+2\tfrac{\partial w}{\partial z}\right),\ \sigma_{xy}=\mu(T)\left(\tfrac{\partial u}{\partial y}+\tfrac{\partial v}{\partial x}\right),\\ \sigma_{xz}=\mu(T)\left(\tfrac{\partial u}{\partial z}+\tfrac{\partial w}{\partial x}\right),\ \sigma_{yz}=\mu(T)\left(\tfrac{\partial w}{\partial y}+\tfrac{\partial v}{\partial z}\right).\end{gathered} \tag{9}$$

We can write the governing equations in curvilinear coordinates as

$$\frac{\partial \hat{\boldsymbol{Q}}}{\partial t}+\frac{\partial \hat{\boldsymbol{F}}}{\partial \xi}+\frac{\partial \hat{\boldsymbol{G}}}{\partial \eta}+\frac{\partial \hat{\boldsymbol{H}}}{\partial \zeta}=\frac{1}{Re}\left(\frac{\partial \hat{\boldsymbol{F}}_v}{\partial \xi}+\frac{\partial \hat{\boldsymbol{G}}_v}{\partial \eta}+\frac{\partial \hat{\boldsymbol{H}}_v}{\partial \zeta}\right), \tag{10}$$

where

$$\begin{gathered}\hat{\boldsymbol{Q}}=\tfrac{\boldsymbol{Q}}{J},\ \hat{\boldsymbol{F}}=\tfrac{\xi_x\boldsymbol{F}+\xi_y\boldsymbol{G}+\xi_z\boldsymbol{H}}{J},\ \hat{\boldsymbol{G}}=\tfrac{\eta_x\boldsymbol{F}+\eta_y\boldsymbol{G}+\eta_z\boldsymbol{H}}{J},\ \hat{\boldsymbol{H}}=\tfrac{\zeta_x\boldsymbol{F}+\zeta_y\boldsymbol{G}+\zeta_z\boldsymbol{H}}{J},\\ \hat{\boldsymbol{F}}_v=\tfrac{\xi_x\boldsymbol{F}_v+\xi_y\boldsymbol{G}_v+\xi_z\boldsymbol{H}_v}{J},\ \hat{\boldsymbol{G}}_v=\tfrac{\eta_x\boldsymbol{F}_v+\eta_y\boldsymbol{G}_v+\eta_z\boldsymbol{H}_v}{J},\ \hat{\boldsymbol{H}}_v=\tfrac{\zeta_x\boldsymbol{F}_v+\zeta_y\boldsymbol{G}_v+\zeta_z\boldsymbol{H}_v}{J}.\end{gathered} \tag{11}$$

The Jacobian J of the coordinate transformation between the curvilinear (ξ, η, ζ) and Cartesian (x, y, z) frames is

$$J = \frac{1}{\begin{vmatrix} 1 & 0 & 0 & 0 \\ 0 & x_\xi & x_\eta & x_\zeta \\ 0 & y_\xi & y_\eta & y_\zeta \\ 0 & z_\xi & y_\eta & z_\zeta \end{vmatrix}}, \tag{12}$$

and

$$\begin{pmatrix} \xi_x & \xi_y & \xi_z \\ \eta_x & \eta_y & \eta_z \\ \zeta_x & \zeta_y & \zeta_z \end{pmatrix} = J \begin{pmatrix} y_\eta z_\zeta - y_\zeta z_\eta & z_\eta x_\zeta - z_\zeta x_\eta & x_\eta y_\zeta - x_\zeta y_\eta \\ y_\zeta z_\xi - y_\xi z_\zeta & z_\zeta x_\xi - z_\xi x_\zeta & x_\zeta y_\xi - x_\xi y_\zeta \\ y_\xi z_\eta - y_\eta z_\xi & z_\xi x_\eta - z_\eta x_\xi & x_\xi y_\eta - x_\eta y_\xi \end{pmatrix}. \tag{13}$$

The reference values for length, density, velocity, temperature, and pressure are δ_{in}, ρ_∞, U_∞, T_∞, and $\rho_\infty U_\infty^2$, respectively, where δ_{in} is the inflow displacement thickness. And the Mach number M_∞ and Reynolds number Re are expressed as

$$M_\infty = \frac{U_\infty}{\sqrt{\gamma R T_\infty}}, \quad Re = \frac{\rho_\infty U_\infty \delta_{in}}{\mu_\infty}, \tag{14}$$

where R is the ideal gas constant, γ the ratio of specific heats, and μ_∞ the viscosity.

The computational grid system employed in our simulation is structured with dimensions of $1920 \times 128 \times 241$, delineating the number of grid points allocated in the streamwise (x), spanwise (y), and wall-normal (z) directions, respectively. A schematic for the spatial domain is displayed in Figure 1. In the wall-normal direction (z), the grid exhibits a stretching characteristic, which is crucial for resolving the boundary layer phenomena near the wall, where gradients can be steep. This stretching allows for a finer resolution close to the wall, enhancing the accuracy of the simulation results in regions where flow behavior is most complex. Conversely, in the streamwise (x) and spanwise (y) directions, the grid is uniformly distributed, ensuring a consistent and systematic approach to capturing the flow characteristics across the computational domain. At the inlet of the simulation, the first grid interval in the wall-normal direction is set to 0.43 wall units ($y^+ = 0.43$). This specific value is strategically chosen to balance the need for resolution in the boundary layer while maintaining computational efficiency.

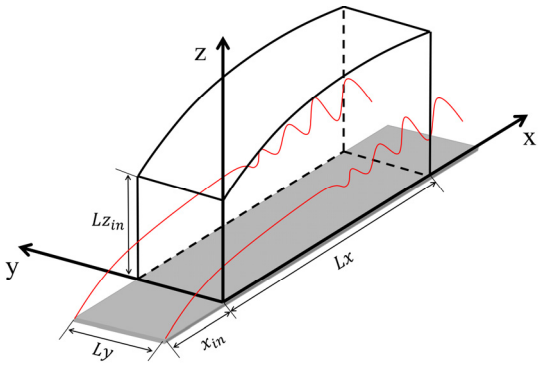

Figure 1. A schematic of the simulation domain.

For a comprehensive understanding of the simulation parameters, Table 1 provides a detailed overview of the geometric parameters, while Table 2 enumerates the flow parameters utilized in our computational study. Key flow parameters include the Mach number, which indicates the flow speed relative to the speed of sound, and the Reynolds number, which characterizes the flow regime and influences the turbulence characteristics of the simulation. Additionally, the variable x_{in} denotes the distance from the leading edge to the inlet. The lengths of the computational domain in the respective directions are represented by Lx, Ly, and Lz_{in}. Lastly, T_w signifies the wall temperature, a crucial factor

influencing heat transfer and flow behavior near the wall. This meticulous setup ensures that the simulation captures the essential physical phenomena with high fidelity.

Table 1. Geometric parameters.

x_{in}	Lx	Ly	Lz_{in}
$300.79\delta_{in}$	$798.03\delta_{in}$	$22\delta_{in}$	$40\delta_{in}$

Table 2. Flow parameters.

M_∞	Re	T_w	T_∞
0.5	1000	273.15 K	273.15 K

The validations of our DNS code can be found in [19,20]. The DNS results are well-verified by comparison with theoretical and experimental data and are consistent with other DNS results [21].

2.3. Artificial Neural Networks

Artificial neural networks (ANNs) represent a sophisticated class of computational models that draw inspiration from the intricate architecture and operational mechanisms of the human brain. These networks are comprised of a multitude of interconnected nodes, commonly referred to as artificial neurons, which are systematically organized into distinct layers. The flow of information within an ANN initiates at the input layer, where raw data are introduced into the system. These data then traverse one or more hidden layers, where complex computations and transformations occur, before culminating in the output layer, which generates the final results.

The training of ANNs is a critical aspect of their functionality, involving sophisticated algorithms designed to optimize the connections between neurons based on empirical data. This training process enables ANNs to discern and learn intricate patterns and relationships inherent in the data, making them exceptionally adept at handling nonlinear relationships and processing vast quantities of information. As a result, ANNs have found extensive applications across diverse domains, including image recognition, natural language processing, and predictive analytics, where their capacity to model complex interactions is invaluable.

In the context of fluid dynamics, flow profiles encapsulate a range of flow variables such as pressure, density, velocity, vorticity, and temperature. Particularly within profile pairs—such as pressure–density and vorticity–velocity—the relationships among these variables exhibit nonlinear characteristics that necessitate the resolution of the Navier–Stokes equations alongside other related parameters. Traditional analytical methods can be cumbersome and computationally intensive; however, the advent of machine learning techniques offers a promising avenue for approximating these nonlinear relationships. Given an adequate volume of training data in the form of flow profile pairs, machine learning models can effectively learn these complex interactions, even in instances where certain variables are not explicitly provided.

In our research methodology, we commence by generating a substantial dataset of profile pairs, which serves as the foundational training data for the neural network. These profile pairs consist of input–output combinations representing various flow variables or parameters, such as pressure–density, vorticity–velocity, or streamwise vorticity–streamwise velocity. To analyze and learn from this dataset, we employ a multilayer perceptron (MLP), a specific architecture of artificial neural networks known for its effectiveness in function approximation.

The MLP undergoes a rigorous training regimen, wherein it iteratively adjusts its internal parameters to minimize the deviation between the predicted outputs and the actual outputs corresponding to the provided inputs. This process involves the application of

advanced optimization techniques aimed at refining the relationship encoded within the nonlinear mathematical model that the MLP embodies. Through this iterative optimization, we enhance the predictive accuracy of the model, enabling it to make reliable forecasts on unseen data or extrapolate to novel flow conditions. Ultimately, this optimized ANN model not only facilitates improved predictive performance but also yields valuable insights into the fundamental physics governing the fluid dynamics of the system under investigation.

3. Numerical Results

The convergence test for different numbers of hidden layers was conducted for each of the following cases, and it showed that the increase in the number of hidden layers will not improve the results much if there are more than three hidden layers for these cases. To balance the resolution and computational cost, four hidden layers were used in each case.

In the context of the Sod shock tube problem and the Shu–Osher problem, computational simulations yield corresponding pressure–density distributions. These profiles serve as the foundational input for an ANN model that forecasts density distributions predicated on pressure input. Furthermore, we conducted a comprehensive analysis of the correlation between mean spanwise vorticity and mean streamwise velocity, as well as the relationship between streamwise vorticity and streamwise velocity.

3.1. Sod Shock Tube Problem

In Figure 2, we showcase a compelling example illustrating the utilization of 1000 pairs of pressure–density profiles, meticulously derived from extensive numerical simulations, to construct a sophisticated ANN model. Within this framework, the pressure profiles were designated as the input data, while the corresponding density profiles were defined as the target outputs that the model was tasked with predicting.

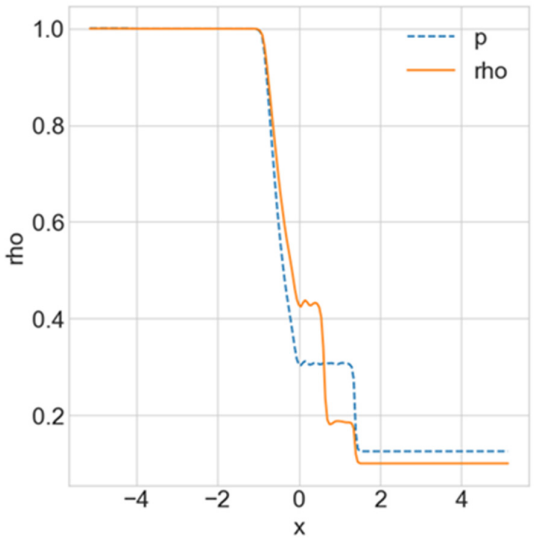

Figure 2. Pressure–density profile pairs (1000 pairs).

Figure 3 further elucidates the model's exceptional capability in discerning and accurately representing the discontinuities and trends present in the profile data, particularly at critical time steps 742 and 851. These specific time points were strategically selected to emphasize instances of abrupt changes within the profiles, which are crucial for understanding the underlying physical phenomena. Upon initial examination, the disparities between the pressure and density profiles, as depicted in Figure 2, appeared to be quite pronounced, indicating a seemingly weak correlation between the two sets of data. This initial observation suggested that the relationship between the input and output variables was not immediately intuitive or easily predictable. However, the ANN model exhibited remarkable robustness and adaptability, successfully capturing these intricate features

embedded within the profiles. The correlation coefficients of the predicted and original profiles at these two time steps reached 0.9994, respectively. The model's prowess in identifying and replicating the discontinuities and trends in the data, despite the initial lack of an apparent correlation, underscores the formidable potential of machine learning techniques in this context. Such techniques are particularly adept at uncovering and interpreting subtle and complex patterns and relationships within datasets, even when these connections may not be readily discernible through conventional analytical methods. This capability not only highlights the ANN model's effectiveness in managing complex and nonlinear relationships but also emphasizes its invaluable utility in a wide range of scientific and engineering applications, where the intricacies of data can often present significant challenges to traditional approaches.

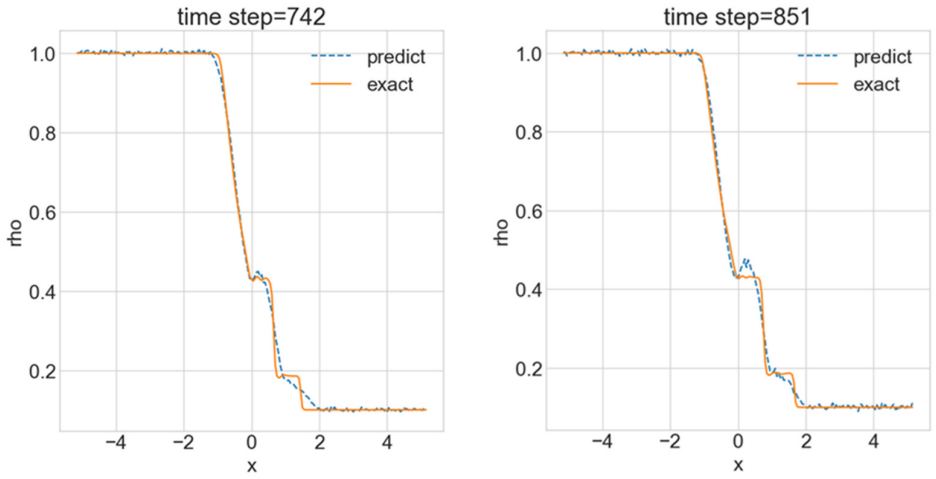

(**a**) (**b**)

Figure 3. Comparison of predicted and exact solutions at (**a**) time step = 742; (**b**) time step = 851.

3.2. Shu–Osher Problem

In Figure 4, we present a comprehensive analysis derived from an extensive dataset comprising 1800 pairs of pressure–density profiles, meticulously generated through sophisticated numerical simulations. This figure serves to illuminate the pronounced and contrasting characteristics that emerge when comparing the density and pressure profiles. Notably, the density profiles reveal intricate small-scale wave patterns, indicative of dynamic fluctuations within the medium. In stark contrast, the pressure profiles appear remarkably stable and devoid of such oscillatory features. This stark divergence between the two profiles suggests a weak correlation (the correlation coefficient reaches infinity for the profiles after the shock at the initial time step), implying that the relationship between pressure and density is neither direct nor straightforward.

To delve deeper into this intriguing phenomenon, we turn our attention to Figure 5, which illustrates the model's predictive capabilities at three distinct time intervals—52, 176, and 426. Despite the evident discrepancies between the pressure and density profiles, our model demonstrated an impressive accuracy in its predictions when juxtaposed with the numerical solutions. It not only adeptly captured the discontinuities present within the profiles but also successfully replicated the small-scale wave patterns observed in the density profiles. The correlation coefficients of the predicted profile and original profile at these three time steps are 0.9978, 0.9971, and 0.9987, respectively. This close correspondence between the model's predictions and the numerical results is particularly remarkable.

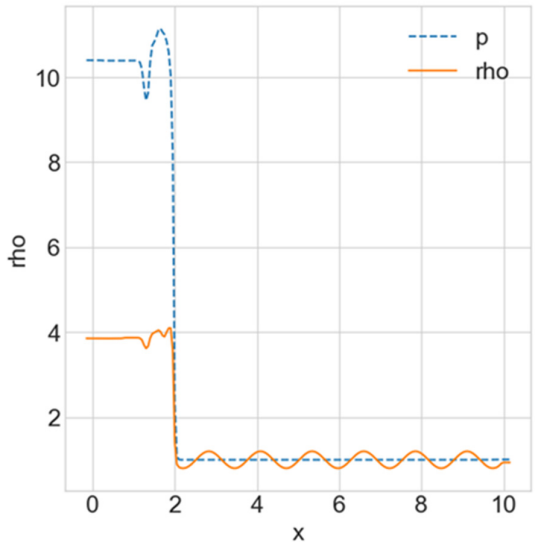

Figure 4. Pressure–density profile pairs (1800 pairs).

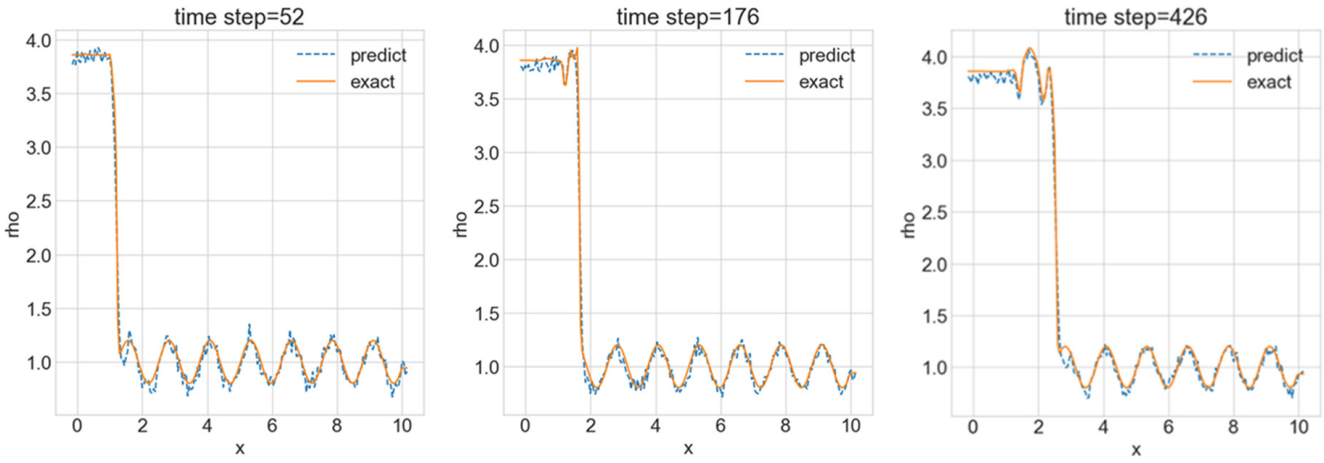

Figure 5. Comparison of predicted and exact solutions at (**a**) time step = 52; (**b**) time step = 176; (**c**) time step = 426.

The significance of this alignment cannot be overstated; it highlights the effectiveness of our machine learning approach in accurately modeling and understanding complex flow dynamics. This achievement transcends the conventional limitations associated with traditional correlation-based analyses, showcasing the potential of advanced computational techniques to unravel the intricacies of fluid behavior in a more nuanced and reliable manner.

3.3. Transitional Boundary Layer

3.3.1. Averaged Spanwise Vorticity (Input) vs. Averaged Streamwise Velocity (Output)

In this part, we employed an ANN to model the relationship between the mean spanwise vorticity profile and the mean streamwise velocity profile. Specifically, we designated the mean spanwise vorticity as the input layer of the network, while the mean streamwise velocity served as the output layer. Despite the relatively modest size of our dataset, comprising only 640 pairs of observations, the results we obtained were remarkably promising.

To enhance our analysis, we strategically selected distance steps of 128 dx, 176 dx, and 516 dx. This choice enabled us to effectively discern and capture trends in the variation in

the data, as illustrated in Figure 6. The successful outcomes of our model underscore the capability of the neural network approach to unravel the intricate relationship between spanwise vorticity and streamwise velocity. It is important to note that while there is a certain degree of correlation between these two variables, the decision to utilize independent variables in modeling could potentially lead to suboptimal results. This observation emphasizes the significance of integrating interconnected variables within machine learning frameworks. By doing so, we can significantly enhance the performance and predictive accuracy of our models, thereby achieving more reliable and insightful outcomes in our analyses.

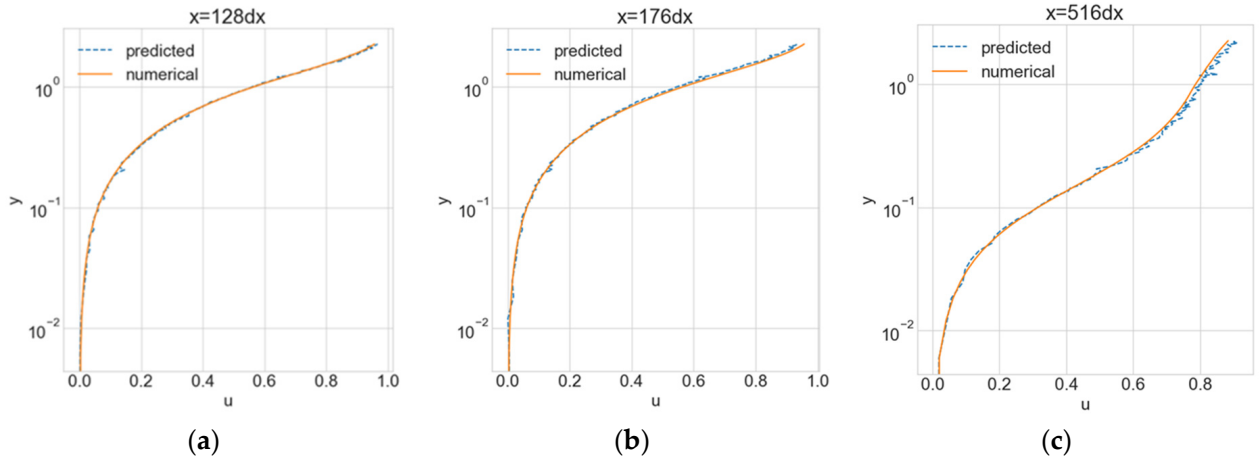

Figure 6. Comparison of predicted and numerical solutions at (**a**) $x = 128\ dx$; (**b**) $x = 176\ dx$; (**c**) $x = 516\ dx$.

3.3.2. Streamwise Vorticity (Input) vs. Streamwise Velocity (Output)

In this part, we employed an ANN to analyze the intricate dynamics of fluid flow by utilizing streamwise vorticity profiles as the input layer and streamwise velocity as the output layer. This innovative approach allowed us to delve into the complex interactions between these two critical parameters.

Interestingly, we observed that when there is a weak correlation between streamwise vorticity and streamwise velocity, the prediction error tends to escalate. The Mean Squared Error (MSE) between the profiles at the three streamwise locations reaches 0.08, 0.08 and 0.11, respectively, while the MSE of the profiles in Figure 6 is less than 10^{-3} for comparison. This phenomenon is illustrated in Figure 7, where we examined distance steps of 130 dx, 205 dx, and 516 dx, each revealing significant discrepancies in the model's predictions.

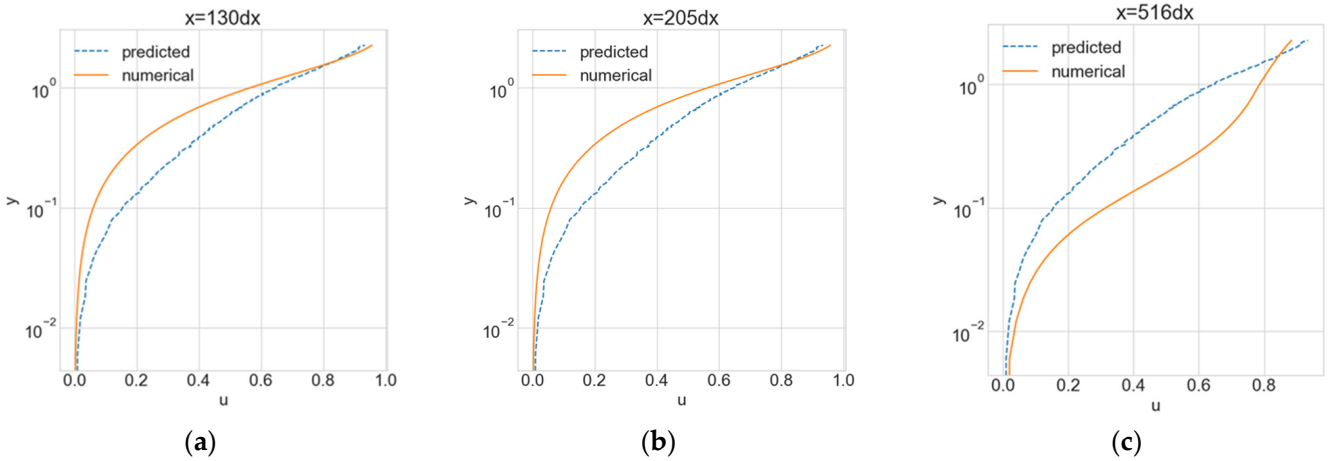

Figure 7. Comparison of predicted and numerical solutions at (**a**) $x = 130\ dx$; (**b**) $x = 205\ dx$; (**c**) $x = 516\ dx$.

Despite this initial challenge posed by the weak correlation, we strategically harnessed this characteristic to enhance our understanding of the flow field's parameters. By integrating both streamwise vorticity and velocity into the training regimen of the neural network, we enabled the model to effectively discern and learn the underlying relationships between these variables. This comprehensive training process facilitated the ANN model's ability to capture the nuanced interplay between streamwise vorticity and velocity, ultimately leading to more accurate predictions. This methodology not only underscores the efficacy of machine learning techniques in revealing hidden patterns and intricate relationships within the realm of complex fluid dynamics but also significantly advances our understanding and predictive capabilities in fluid mechanics.

4. Conclusions

This comprehensive study delves into the innovative application of ANNs to unravel the intricate nonlinear behaviors exhibited in complex fluid flows. By leveraging flow profile pairs meticulously generated from numerical simulations of well-established benchmark cases—most notably the one-dimensional Sod tube problem and the Shu–Osher problem—this research demonstrates how ANNs can adeptly capture critical features such as discontinuities and small-scale waves, which are quintessential characteristics of complex fluid dynamics. The findings reveal that in transitional flow scenarios, the predictions made by the ANN exhibit remarkable congruence with results obtained from DNS. This alignment not only underscores the ANN's proficiency in modeling complex flow behaviors but also emphasizes its ability to track the nuanced evolution of flow profiles over time. Such capabilities are essential for understanding the dynamics of fluid flows that are often subject to rapid changes and intricate interactions.

Moreover, this study accentuates the transformative potential of machine learning methodologies in enhancing our comprehension of complex fluid dynamics phenomena. By showcasing the utility of ANNs across a variety of flow scenarios, the research provides valuable insights into the intricate correlations that exist among different flow parameters. This ability to discern relationships between variables is pivotal for advancing predictive modeling in fluid dynamics.

The integration of numerical simulation with machine learning techniques marks a significant step forward in the development of more accurate and insightful models. These models are not only capable of predicting fluid behavior with greater precision but also serve as powerful analytical tools in both engineering and scientific contexts. In summary, this study illustrates the substantial promise held by machine learning approaches, particularly artificial neural networks, in propelling our understanding of complex fluid dynamics.

Author Contributions: Conceptualization and methodology, S.Y., C.C., Y.Y. (Yong Yang) and Y.Y. (Yonghua Yan); formal analysis, S.Y., C.C., Y.Y. (Yong Yang) and Y.Y. (Yonghua Yan); writing—original draft preparation, S.Y. and Y.Y. (Yonghua Yan); writing—review and editing, Y.Y. (Yong Yang), Y.Y. (Yonghua Yan) and C.C.; visualization, C.C. and Y.Y. (Yonghua Yan). All authors have read and agreed to the published version of the manuscript.

Funding: This research was supported by the Mississippi NASA EPSCoR program.

Data Availability Statement: Data are contained within the article.

Acknowledgments: This work relied on computations performed on the WTAMU HPC cluster, which was funded by the National Science Foundation (NSF CC* GROWTH 2018841).

Conflicts of Interest: The authors declare no conflicts of interest.

References

1. Brunton, S.L.; Noack, B.R.; Koumoutsakos, P. Machine Learning for Fluid Mechanics. *Annu. Rev. Fluid Mech.* **2020**, *52*, 477–508. [CrossRef]
2. Shi, E.; Xu, C. A Comparative Investigation of Neural Networks in Solving Differential Equations. *J. Algorithms Comput. Technol.* **2021**, *15*, 174830262199860. [CrossRef]
3. LeCun, Y.; Bengio, Y.; Hinton, G. Deep Learning. *Nature* **2015**, *521*, 436–444. [CrossRef] [PubMed]

4. Kutz, J.N. Deep Learning in Fluid Dynamics. *J. Fluid Mech.* **2017**, *814*, 1–4. [CrossRef]
5. Raghu, M.; Schmidt, E. A Survey of Deep Learning for Scientific Discovery. *arXiv* **2020**, arXiv:2003.11755.
6. Morimoto, M.; Fukami, K.; Zhang, K.; Fukagata, K. Generalization Techniques of Neural Networks for Fluid Flow Estimation. *Neural Comput. Appl.* **2022**, *34*, 3647–3669. [CrossRef]
7. Razdan, S.; Shah, S. Optimization of Fluid Modeling and Flow Control Processes Using Machine Learning: A Brief Review. In *Advances in Mechanical Engineering and Material Science*; Popat, K.C., Kanagaraj, S., Sreekanth, P.S.R., Kumar, V.M.R., Eds.; Lecture Notes in Mechanical Engineering; Springer Nature: Singapore, 2022; pp. 63–85; ISBN 978-981-19067-5-6.
8. Mendez, M.A.; Dominique, J.; Fiore, M.; Pino, F.; Sperotto, P.; van den Berghe, J. Challenges and Opportunities for Machine Learning in Fluid Mechanics. *arXiv* **2022**, arXiv:2202.12577.
9. Roy, P.; Tamang, S.K.; Das, S.; Rajasekaran, T. *An Application of Deep Neural Network Using GNS for Solving Complex Fluid Dynamics Problems: In Advances in Systems Analysis, Software Engineering, and High Performance Computing*; Thanigaivelan, R., Suchithra, M., Kaliappan, S., Mothilal, T., Eds.; IGI Global: Hershey, PA, USA, 2024; pp. 1–22. ISBN 9798369333143.
10. Khan, M.; Imran, M.; Khan, W. A Neural Network Approach to Modeling Magnetohydrodynamic Stagnation Point Ree-Eyring Flow over a Convectively Heated Stretched Surface. *Int. J. Model. Simul.* **2024**, 1–14. [CrossRef]
11. Morra, P.; Meneveau, C.; Zaki, T.A. ML for Fast Assimilation of Wall-Pressure Measurements from Hypersonic Flow over a Cone. *Sci. Rep.* **2024**, *14*, 12853. [CrossRef] [PubMed]
12. Guo, X.; Li, W.; Iorio, F. Convolutional Neural Networks for Steady Flow Approximation. In Proceedings of the 22nd ACM SIGKDD International Conference on Knowledge Discovery and Data Mining, San Francisco, CA, USA, 13 August 2016; pp. 481–490.
13. Ribeiro, M.D.; Rehman, A.; Ahmed, S.; Dengel, A. DeepCFD: Efficient Steady-State Laminar Flow Approximation with Deep Convolutional Neural Networks. *arXiv* **2021**, arXiv:2004.08826.
14. Jin, X.; Cai, S.; Li, H.; Karniadakis, G.E. NSFnets (Navier-Stokes Flow Nets): Physics-Informed Neural Networks for the Incompressible Navier-Stokes Equations. *J. Comput. Phys.* **2021**, *426*, 109951. [CrossRef]
15. Portal-Porras, K.; Fernandez-Gamiz, U.; Ugarte-Anero, A.; Zulueta, E.; Zulueta, A. Alternative Artificial Neural Network Structures for Turbulent Flow Velocity Field Prediction. *Mathematics* **2021**, *9*, 1939. [CrossRef]
16. Sod, G.A. A Survey of Several Finite Difference Methods for Systems of Nonlinear Hyperbolic Conservation Laws. *J. Comput. Phys.* **1978**, *27*, 1–31. [CrossRef]
17. Shu, C.-W.; Osher, S. Efficient Implementation of Essentially Non-Oscillatory Shock-Capturing Schemes. *J. Comput. Phys.* **1988**, *77*, 439–471. [CrossRef]
18. Shu, C.-W.; Osher, S. Efficient Implementation of Essentially Non-Oscillatory Shock-Capturing Schemes, II. *J. Comput. Phys.* **1989**, *83*, 32–78. [CrossRef]
19. Jiang, L.; Chang, C.-L.; Choudhari, M.; Liu, C. Cross-Validation of DNS and PSE Results for Instability-Wave Propagation in Compressible Boundary Layers Past Curvilinear Surfaces. In Proceedings of the 16th AIAA Computational Fluid Dynamics Conference; American Institute of Aeronautics and Astronautics, Orlando, FL, USA, 23 June 2003.
20. Liu, C.; Chen, L. Parallel DNS for Vortex Structure of Late Stages of Flow Transition. *Comput. Fluids* **2011**, *45*, 129–137. [CrossRef]
21. Lee, C.; Li, R. Dominant Structure for Turbulent Production in a Transitional Boundary Layer. *J. Turbul.* **2007**, *8*, N55. [CrossRef]